REPORT DOCUMENTATION PAGE

Form Approved OMB NO. 0704-0188

1. REPORT DATE (DD-MM-YYYY)	2. REPORT TYPE	3. DATES COVERED (From - To)
01-06-2021	Final Report	1-Apr-2017 - 31-Oct-2020

4. TITLE AND SUBTITLE
Final Report: Nano- and Micro-scale Patterning of Virus Assembled Enzymatic Cascades for Bio-Energy Harvesting

5a. CONTRACT NUMBER
W911NF-17-1-0137

5b. GRANT NUMBER

5c. PROGRAM ELEMENT NUMBER
611102

6. AUTHORS

5d. PROJECT NUMBER

5e. TASK NUMBER

5f. WORK UNIT NUMBER

7. PERFORMING ORGANIZATION NAMES AND ADDRESSES
University of Maryland - College Park
Office of Research Administration
3112 Lee Building 7809 Regents Drive
College Park, MD 20742 -5141

8. PERFORMING ORGANIZATION REPORT NUMBER

9. SPONSORING/MONITORING AGENCY NAME(S) AND ADDRESS (ES)
U.S. Army Research Office
P.O. Box 12211
Research Triangle Park, NC 27709-2211

10. SPONSOR/MONITOR'S ACRONYM(S)
ARO

11. SPONSOR/MONITOR'S REPORT NUMBER(S)
70938-LS.13

12. DISTRIBUTION AVAILIBILITY STATEMENT
Approved for public release; distribution is unlimited.

13. SUPPLEMENTARY NOTES
The views, opinions and/or findings contained in this report are those of the author(s) and should not contrued as an official Department of the Army position, policy or decision, unless so designated by other documentation.

14. ABSTRACT

15. SUBJECT TERMS

16. SECURITY CLASSIFICATION OF:			17. LIMITATION OF ABSTRACT	15. NUMBER OF PAGES	19a. NAME OF RESPONSIBLE PERSON
a. REPORT	b. ABSTRACT	c. THIS PAGE			James Culver
UU	UU	UU	UU		19b. TELEPHONE NUMBER 301-405-2912

RPPR Final Report
as of 02-Jun-2021

Agency Code: 21XD

Proposal Number: 70938LS **Agreement Number: W911NF-17-1-0137**
INVESTIGATOR(S):

Name: James N. Culver
Email: culver@ibbr.umd.edu
Phone Number: 3014052912
Principal: Y

Organization: **University of Maryland - College Park**
Address: Office of Research Administration, College Park, MD 207425141
Country: USA
DUNS Number: 790934285 EIN: 526002033

Report Date: 31-Jan-2021 Date Received: 01-Jun-2021
Final Report for Period Beginning 01-Apr-2017 and Ending 31-Oct-2020
Title: Nano- and Micro-scale Patterning of Virus Assembled Enzymatic Cascades for Bio-Energy Harvesting
Begin Performance Period: 01-Apr-2017 **End Performance Period:** 31-Oct-2020
Report Term: 0-Other

Submitted By: James Culver Email: culver@ibbr.umd.edu
Phone: (301) 405-2912

STEM Degrees: 2 **STEM Participants:** 4

Major Goals: There is enormous potential in the development of in vitro enzyme catalytic systems for the production of chemicals, materials and energy that could not otherwise be produced using existing technologies. However, to realize this potential new approaches for the development and deployment of biocatalysts are needed. Specific challenges in this area include the need for 1) enhanced portfolios of ready-to-use enzymes, 2) tunable multi-enzyme cascades, 3) platforms for the spatial organization of enzymes, and 4) scalable device interface systems to control and monitor enzyme activities. Efforts in this proposal will address challenge areas involving the spatial organization of biocatalysts within controllable microsystems. Our goals are to develop the knowledge needed to modulate and optimize the spatial organization of enzyme cascade activities at the interface between biology and electronic devices. To address these challenges our team has developed TMV- based nano-scaffolds for the molecular patterning of enzymes as well as microfluidic systems for the controlled assembly of these scaffolds onto electrode surfaces. Specific efforts will 1) investigate TMV- VLP structure and assembly modifications required to promote nanoscale enzyme patterning on the VLP nanorod surface, 2) develop and characterize systems to efficiently interface VLP-patterned biofuel enzymes onto electrode surfaces, and 3) examine microfluidic systems for the controlled microscale compartmentalization of VLP-patterned enzymes for enhanced bioenergy generation. When combined, results from these studies will provide fundamental information on the effects of enzyme cascade patterning and electrode interfacing to enhance in vitro biofuel cell activity. It is also anticipate that the information and systems developed in this study will be broadly applicable to an array of enzymatic cascades, providing a universal platform for testing and optimizing portfolios of biocatalyst.

Accomplishments: See Attached Document

Training Opportunities: Post-doctoral, graduate, undergraduate and high school students have participated in aspects of this team-oriented cross-disciplinary project that involves expertise in biology and protein engineering (Dr. Culver) with micro-electro-mechanical systems (MEMS) and microfabrication (Dr. Ghodssi) to develop the knowledge base needed to design, control and assemble complex functionalized macromolecules via microfluidics. Project specific training / professional development activities have included attendance at conferences and seminars and participation in joint laboratory meetings for the dissemination of project results and discussion of experimental plans.

Results Dissemination: Nothing to Report

Honors and Awards: Nothing to Report

RPPR Final Report
as of 02-Jun-2021

Protocol Activity Status:

Technology Transfer: Nothing to Report

PARTICIPANTS:

Participant Type: PD/PI
Participant: James Culver
Person Months Worked: 1.00 **Funding Support:**
Project Contribution:
National Academy Member: N

Participant Type: Co PD/PI
Participant: Reza Ghodssi
Person Months Worked: 1.00 **Funding Support:**
Project Contribution:
National Academy Member: N

Participant Type: Postdoctoral (scholar, fellow or other postdoctoral position)
Participant: Sangwook Chu
Person Months Worked: 6.00 **Funding Support:**
Project Contribution:
National Academy Member: N

Participant Type: Postdoctoral (scholar, fellow or other postdoctoral position)
Participant: Madhu Kappagantu
Person Months Worked: 4.00 **Funding Support:**
Project Contribution:
National Academy Member: N

Participant Type: Graduate Student (research assistant)
Participant: Brown Adam
Person Months Worked: 6.00 **Funding Support:**
Project Contribution:
National Academy Member: N

Participant Type: Graduate Student (research assistant)
Participant: Joanna Avery
Person Months Worked: 1.00 **Funding Support:**
Project Contribution:
National Academy Member: N

Participant Type: Undergraduate Student
Participant: Matthew Brandon
Person Months Worked: 1.00 **Funding Support:**

RPPR Final Report
as of 02-Jun-2021

Project Contribution:
National Academy Member: N

Participant Type: High School Student
Participant: Feroz Campbell
Person Months Worked: 1.00 **Funding Support:**
Project Contribution:
National Academy Member: N

ARTICLES:

Publication Type: Journal Article Peer Reviewed: Y **Publication Status:** 1-Published
Journal: Langmuir
Publication Identifier Type: DOI Publication Identifier: 10.1021/acs.langmuir.7b02920
Volume: 34 Issue: 4 First Page #: 1725
Date Submitted: 8/21/18 12:00AM Date Published: 1/1/18 10:00AM
Publication Location:
Article Title: Localized Three-Dimensional Functionalization of Bionanoreceptors on High-Density Micropillar Arrays via Electrowetting
Authors: Sangwook Chu, Thomas E. Winkler, Adam D. Brown, James N. Culver, Reza Ghodssi
Keywords: Macromolecule, Bioprinting
Abstract: In this work, we introduce an electrowetting- assisted 3-D biofabrication process allowing both complete and localized functionalization of bionanoreceptors onto densely arranged 3-D microstructures. The integration of biomaterials with 3-D microdevice components offers exciting opportunities for communities developing miniature bioelectronics with enhanced performance and advanced modes of operation. However, most biological materials are stable only in properly conditioned aqueous solutions, thus the water-repellent proper- ties exhibited by densely arranged micro/nanostructures (widely known as the Cassie?Baxter state) represent a significant challenge to biomaterial integration. Here, we first investigate such potential limitations using cysteine-modified tobacco mosaic virus (TMV1cys) as a model bionanoreceptor and a set of Au-coated Si-micropillar arrays (?PAs) of varying densities. Furthermore, we introduce a novel biofabrication system adopting electrowetting principles for the
Distribution Statement: 3-Distribution authorized to U.S. Government Agencies and their contractors
Acknowledged Federal Support: **Y**

RPPR Final Report
as of 02-Jun-2021

Publication Type: Journal Article Peer Reviewed: Y **Publication Status:** 1-Published
Journal: Biotechnology Journal
Publication Identifier Type: DOI Publication Identifier: 10.1002/biot.201800147
Volume: 13 Issue: 12 First Page #: 1
Date Submitted: 8/20/19 12:00AM Date Published:
Publication Location:
Article Title: Tobacco Mosaic Virus as a Versatile Platform for Molecular Assembly and Device Fabrication
Authors: Sangwook Chu, Adam Brown, James Culver, Reza Ghodssi
Keywords: Tobacco mosaic virus, Biological template, biofabrication
Abstract: Viruses are unique biological agents that infect living host cells through molecular delivery of a genomic cargo. Over the past two decades advancements in genetic engineering and bioconjugation technologies have allowed the unprecedented use of these “unfriendly” biological molecules, as nanoscopic platforms for the advancement of an array of nanotechnology applications. This mini-review focuses on providing a brief summary of key demonstrations leveraging the versatile characteristics of Tobacco mosaic virus (TMV) for molecular assembly and bio-device integration. A comprehensive discussion of genetic and chemical modification strategies along with potential limiting factors that impact the assembly of these macromolecules is presented to provide useful insights for adapting TMV as a potentially universal platform towards developing advanced nanomaterials. Additional discussions on biofabrication techniques developed in parallel to enable immobilization, alignment, and patterning of
Distribution Statement: 3-Distribution authorized to U.S. Government Agencies and their contractors
Acknowledged Federal Support: **Y**

CONFERENCE PAPERS:

Publication Type: Conference Paper or Presentation **Publication Status:** 0-Other
Conference Name: FNANO
Date Received: 24-Aug-2018 Conference Date: 15-Apr-2018 Date Published: 15-Apr-2018
Conference Location: Snowbird, UT
Paper Title: Directed self-assembly of environmentally responsive virus-like nanoscaffolds
Authors: Adam D. Brown, Sangwook Chu, Reza Ghodssi, James N. Culver
Acknowledged Federal Support: **Y**

Publication Type: Conference Paper or Presentation **Publication Status:** 0-Other
Conference Name: Materials Research Society
Date Received: 24-Aug-2018 Conference Date: 26-Nov-2017 Date Published: 26-Aug-2018
Conference Location: Boston, MA
Paper Title: Virus-Assisted Immobilization of Glucose Oxidase for High Power Enzymatic Biofuel Cells
Authors: Sangwook Chu, Pradeep Rajasekaran, James N. Culver, Reza Ghodssi
Acknowledged Federal Support: **Y**

Publication Type: Conference Paper or Presentation **Publication Status:** 0-Other
Conference Name: Hilton Head Solid-State Sensors, Actuators and Microsystems Workshop
Date Received: 24-Aug-2018 Conference Date: 03-Jun-2018 Date Published: 03-Jun-2018
Conference Location: Hilton Head, SC
Paper Title: PRINTING BIOLOGICAL LIQUID ON HYDROPHOBIC 3D ELECTRODES
Authors: S. Chu, M.J. Lerman, J.N. Culver, J.P. Fisher, R. Ghodssi
Acknowledged Federal Support: **Y**

RPPR Final Report
as of 02-Jun-2021

Publication Type: Conference Paper or Presentation **Publication Status:** 0-Other
Conference Name: Microtechnologies in Medicine
Date Received: 24-Aug-2018 Conference Date: 26-Mar-2018 Date Published: 26-Mar-2018
Conference Location: Monterey, CA
Paper Title: ELECTROWETTING FOR BIO-PRINTING ON 3D HYDROPHOBIC ELECTRODES
Authors: S. Chu, M.J. Lerman, J.N. Culver, J.P. Fisher, R. Ghodssi
Acknowledged Federal Support: **Y**

Publication Type: Conference Paper or Presentation **Publication Status:** 1-Published
Conference Name:
Date Received: Conference Date: 04-Dec-2018 Date Published: 04-Dec-2018
Conference Location: Daytona Beach FL
Paper Title: Virus-assembled technology for next generation bioenergy harvesting devices
Authors: Sangwook Chu, Adam D Brown, James N Culver, Reza Ghodssi
Acknowledged Federal Support: **Y**

Publication Type: Conference Paper or Presentation **Publication Status:** 1-Published
Conference Name: Transducers
Date Received: 21-Aug-2020 Conference Date: 22-Jun-2019 Date Published: 22-Jun-2019
Conference Location: Berlin, Germany
Paper Title: A SCALABLE 3-D PRINTED BIOLOGICAL ASSEMBLY TECHNOLOGY
Authors: Sangwook Chu, Adam D. Brown, James N. Culver, Reza Ghodssi
Acknowledged Federal Support: **Y**

Publication Type: Conference Paper or Presentation **Publication Status:** 1-Published
Conference Name: Transducers
Date Received: 21-Aug-2020 Conference Date: 22-Jun-2019 Date Published: 22-Jun-2019
Conference Location: Berlin, Germany
Paper Title: BIONANOSCAFFOLDS-ENABLED NON-WETTING SURFACES FOR ANTIBIOFOULING APPLICATIONS
Authors: Sangwook Chu, Ishita Shahi, Ryan C Huiszoon, James N Culver, Reza Ghodssi
Acknowledged Federal Support: **Y**

DISSERTATIONS:

Publication Type: Thesis or Dissertation
Institution: University of Maryland
Date Received: 24-Aug-2018 Completion Date: 8/16/18 8:53PM
Title: THREE-DIMENSIONAL BIOPATTERNING TECHNOLOGY AND APPLICATION FOR ENZYME-BASED BIOELECTRONICS
Authors: Sangwook, Chu
Acknowledged Federal Support: **Y**

Publication Type: Thesis or Dissertation
Institution: University of Maryland, College Park
Date Received: 22-Aug-2019 Completion Date: 12/12/18 8:44PM
Title: 3D ENGINEERING OF VIRUS-BASED PROTEIN NANOTUBES AND RODS: A TOOLKIT FOR GENERATING NOVEL NANOSTRUCTURED MATERIALS
Authors: Adam Degen Brown
Acknowledged Federal Support: **Y**

RPPR Final Report
as of 02-Jun-2021

Partners

,

I certify that the information in the report is complete and accurate:
Signature: James Culver
Signature Date: 6/1/21 11:39AM

Final Report: W911NF1710137

Nano- and Micro-Scale Patterning of Virus Assembled Enzymatic Cascades for Bio-Energy Harvesting

Culver / Ghodssi, University of Maryland

Introduction:

There is enormous potential in the development of *in vitro* enzyme catalytic systems for the production of chemicals, materials and energy. However, to achieve this potential, scalable systems for the spatial organization of enzymes within a microdevice are needed. Efforts in this project have investigated the use of virus-based microfluidic systems to control, pattern and enhance enzyme-based energy production.

Aim 1. TMV-VLP based nanoscale enzyme patterning. Studies in this aim investigated methods for the directed assembly of segmented tobacco mosaic like particles (TMV-VLPs) as a means to pattern selected enzymes across the surface of VLP nanorods. Specific accomplishments include:

1. Charge-Charge Modifications for Directed Nanorod Assembly. The ability of the TMV axial carboxylate group to control VLP assembly was investigated as a means to control CP self-assembly. Initial modifications were directed toward the creation of novel salt bridges between the E50 and D77 carboxylate pairs through replacements with either D77K or E50K (Figure 1A). Interestingly, the D77K substitution resulted in the assembly of rod shaped VLPs (Figure 1B). Structural modeling of D77K indicated sufficient rotational space within the subunit interface at residue 77 to accommodate the lysine residue with its terminal amine group positioned within 3 Å of an opposing E50 carboxyl group from a neighboring subunit. The close approach of the D77K to E50 interaction would result in a new intersubunit salt bridge that is of sufficient strength to drive VLP assemble.

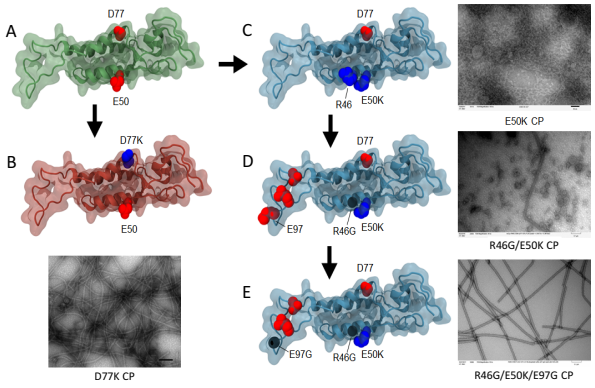

Figure 1. Locations of TMV CP modifications with corresponding micrographs of assembly products. (A) Unmodified TMV CP containing negatively charged axial carboxylates D77 and E50. (B) The D77K CP alone can induce rod production. (C) The E50K substitution fails to produce rods likely due to repulsive interactions with neighboring R46. (D) The R46G/E50K substitutions negate this repulsive interaction, allowing limited rod-like assembles. (E) The addition of an E97G modification aimed at enhancing lateral intersubunit interactions produces R46G/E50K/E97G CP that induces virus-like rod production.

In contrast, the E50K replacement did not produce helical rod assemblies (Figure 1C). Structural modeling indicates the potential for repulsive electrostatic interference between the lysine substituted for residue E50 and residue R46 situated on the adjacent α-helical turn in the same subunit. To eliminate the presumed electrostatic interference of R46 and to accommodate the E50K substitution an additional substitution of glycine for R46 was made, generating the R46G/E50K CP variant. Expression of this variant produced only limited rod assemblies suggesting incomplete compensation of the E50K substitution (Figure 1D). To improve assembly stability and VLP formation, a third targeted substitution, E97G, aimed at partially neutralizing the laterally interacting intersubunit

carboxylates present in the long inner loop was added to create R46G/E50K/E97G. The E97G substitution stabilizes the long inner loop in a virion-like configuration that promotes the helical ordering of subunits necessary for rod assembly [1, 2]. This triple mutant was found to produce VLP nanorods in quantities and lengths (>1 μm) that were similar to those observed for D77K mutation (Figure 1E). This is consistent with the stabilization of the rod assembly via the new axially placed intersubunit salt-bridge and stabilized CP long inner loop.

2. Reprogrammed Carboxylate Interactions with Unique Assembly / Disassembly Profiles. Analysis of the D77K and R46G/E50K/E97G CP assembly profiles identified that each has a unique environmental response. Specifically, the D77K mutation disassembles at pH 9 while the TMV and VLP E50Q/D77N rods remain assembled under this elevated pH condition (Figure 2). Additionally, restoring the disassembled D77K CP solution to pH 7 solution conditions results in the reassembly of the nanorods. Similarly, the R46G/E50K/E97G mutant CP also displays a unique disassembly behavior in response to ionic strength. At low salt concentration, the R46G/E50K/E97G CP disassembles but can then rapidly reassemble upon restoration of the solution's ionic strength. Interestingly, the conditions that trigger disassembly in each of these CP variants in solution is not shared by the other. D77K VLP nanorods are primarily affected by pH and not by ionic strength while the R46G/E50K/E97G nanorods show disassembly only at low ionic strength with pH having little effect (Figure 2). This variation in required assembly conditions makes these CPs potentially useful components for the controlled assembly of chimeric VLPs.

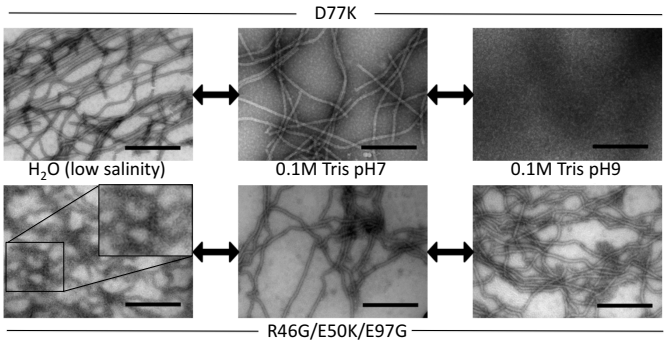

Figure 2. Unique differences in the solution assembly charateristics of carboxylate-altered CPs. (A) D77K-HA and (B) R46G/E50K/E97G-FLAG TEM images showing both variants exist in an assembled state as elongated VLP rods after dialysis in 0.1 M pH 7 Tris (center images). After dialysis with filtered water D77K-HA CP shows retention of assembled VLP structure (top left), while R46G/E50K/E97G-FLAG shows significant loss of assembly structure (bottom left with magnified box). In contrast, dialysis of the samples from 0.1 M pH 7 Tris (center column) to pH 9 (right column) triggers the complete loss of virus-like particle structure in D77K-HA CP (top right), while R46G/E50K/E97G-FLAG CP retains its assembly structure. Bars = 200 nm

It's likely that the pH-based disassembly of D77K VLP results from the deprotonation and subsequent loss of positive charge of the lysine sidechain's primary amine in alkaline conditions around pH 9. The pKa of this amine group in a dilute solution of free lysine is ~10.5 [3]. However, this value can change considerably depending on the local microenvironment of the amine group in the folded protein and within the assembled rod. A similar deprotonation of the lysine in R46G/E50K/E97G CP may also occur, however the partial neutralization of the lateral intersubunit interaction via the E97G substitution likely negates the impact of the engineered axial salt bridge resulting in the relative stability of this CP at pH 9.

For the ionic strength-based disassembly of R46G/E50K/E97G CP, structural modeling indicates that the predicted assembly-promoting salt-bridge between the introduced lysine and the axially oriented carboxylate on the opposing subunit could be additionally stabilized by dissolved ions. While the side chain of the E50K substitution is thought to provide a stabilizing force when interacting with D77 of the opposing subunit,

the E50K lysine is also positioned to interact with R71 of the opposing subunit, generating a repulsive interaction. This repulsive interaction may be mitigated by an ion screening effect when sufficient negative ions are present, allowing the ionic strength of the solution to control the assembly of this nanorod. The D77K lysine, however, does not interact across an intersubunit boundary with R71, and therefore VLP assembly would not be expected to depend on dissolved ions for charge screening.

3. Directed Assembly of Chimeric Nanorods. The unique pH and ionic strength assembly profiles of D77K and R46G/E50K/E97G, respectively, were investigated as a means to produce chimeric virus particles. For these experiments, the D77K mutant was genetically labeled with a C-terminal HA peptide tag while the R46G/E50K/E97G mutant was similarly labeled using a FLAG peptide tag. Solutions containing unlabeled TMV and modified CP VLPs were combined and dialyzed against solution conditions that promote disassembly of the modified CP VLPs. For D77K-HA VLP, this entailed dialysis to pH 9 and for R46G/E50K/E97G-FLAG dialysis against filtered water adjusted to pH 7. Disassembled CPs were then mixed with TMV virions and buffer conditions adjusted back to pH 7 or increased salinity (0.3M NaCl) by dialysis to initiate reassembly of the D77K-HA or R46G/E50K/E97G-FLAG CP, respectively. Samples were then immunolabeled with anti-FLAG or anti-HA antibodies and imaged by electron microscopy.

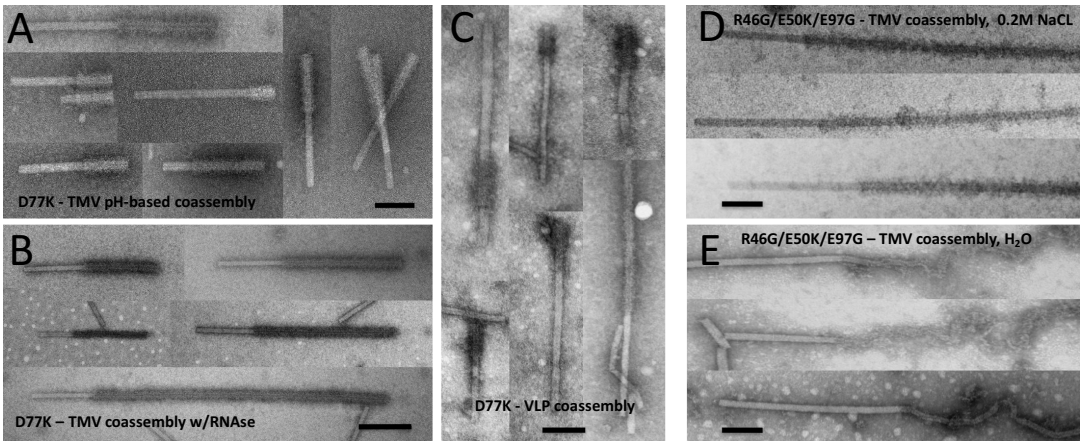

Figure 3. Solution directed coassembly of carboxylate-altered CPs. (A) TEM images of longitudinally ordered TMV– D77K-HA hybrid nanorods resulting from pH-based VLP disassembly / reassembly. Samples were dialysis against a pH 9 solution of 0.1 M Tris buffer and then back to pH 7 followed by immunolabeling with anti-HA antibody. (B) RNAase treated TMV prior to pH directed assembly with D77K-HA CP indicating that any exposure of the viral 5' end RNA is not required for coassembly. (C) D77K-HA CP assembled onto a RNA-free VLP based nanorod produced by the neutralization of the lateral carboxylate cluster, further demonstrating that the viral RNA is not required for coassembly. (D) TEM images of ionic-strength-based R46G/E50K/E97G-FLAG coassembly with TMV. Samples were dialyzed against deionized water and then back to 0.2M NaCl followed by immunolabeling with anti-FLAG antibody. (E) Coassembled TMV with R46G/E50K/E97G-FLAG washed with deionized water after immunolabeling showing loss of VLP assembly structure. Bars = 200 nm

Results from the coassembly of D77K-HA CP and TMV clearly show consistent and efficient assembly of D77K-HA CP onto the unlabeled TMV (Figure 3A and B). The resulting hybrid unlabeled TMV – D77K-HA VLP nanorods showed a range of lengths and were selectively segregated into unlabeled and labeled sections by the anti-HA antibodies. It is likely that strength of the mutant CP – CP interactions combined with CP concentration are factors affecting the observed length of the hybrid nanorod. In addition, such pH treatments have been shown to expose the 5' end of the viral RNA, which functions as a

ribosome binding site during viral infection [1]. To determine if exposure of the 5' end of the virus RNA genome during dialysis plays a role in the coassembly of chimeric D77K-HA nanorods, RNase A was added to the TMV samples prior to coassembly and immunolabeling (Figure 3B). Results revealed the presence of similar end-assembled chimeric nanorods indicating the genomic RNA is not required for the observed coassembly. To further determine if the viral genomic RNA contributes to the observed chimeric nanorod assembly the D77K-HA CP was coassembled onto a RNA-free VLP produced by the neutralization of the lateral carboxylate cluster through CP amino acid substitutions E106Q/E95Q/E97Q/D109N. The D77K-HA was found to assemble onto the E106Q/E95Q/E97Q/D109N VLP in a manner similar to that observed using TMV virions or TMV RNase A treated virions (Figure 3A, B and C). Thus, genomic viral RNA is not required for the coassembly of these CPs. Coassembly of R46G/E50K/E97G-FLAG CP onto TMV by the depletion and subsequent replenishment of dissolved ions also produced chimeric nanorods (Figure 3C). Interestingly, washing the electron microscopy grids containing the coassembled TMV - R46G/E50K/E97G-FLAG CP with deionized water pH 7 resulted in the R46G/E50K/E97G-FLAG CP section exhibiting a loose and fragmented structure consistent

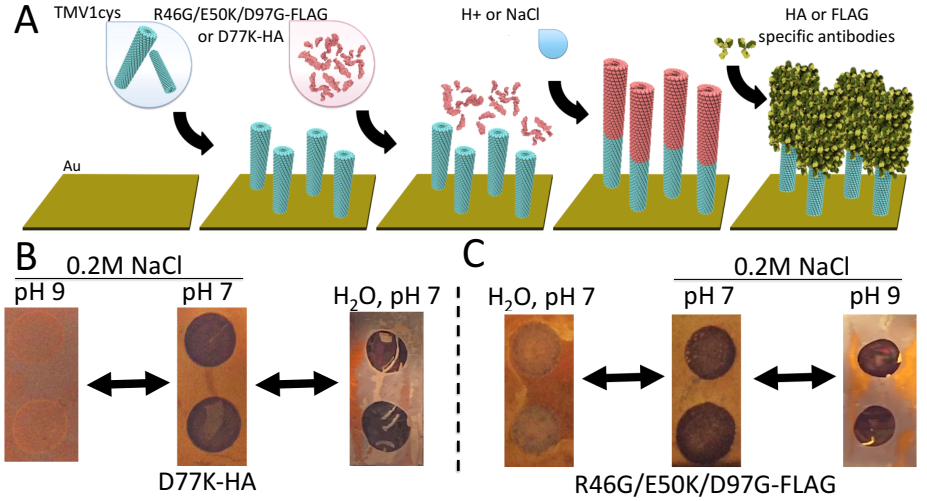

Figure 4. Controlled surface assembly of carboxylate-altered CPs. (A) Diagram displaying assembly steps for the pH or NaCl directed coassembly of D77K-HA and R46G/E50K/E97G-FLAG onto surface attached TMV1cys. In step one TMV1cys is end attached to gold coated silicon chip via a thiol – gold bond. In step two, disassembled carboxylate modified CPs are added to the TMV1cys attached chips. Step three involves the incubation of disassembled CPs under specific pH and salt buffer conditions that promote CP assembly onto the exposed end of attached TMV1cys. Step four demonstrates the addition of primary tag specific antibody (FLAG or HA) followed by the addition of secondary alkaline phosphatase conjugated antibody that upon substrate addition produces a dark pitant precion the surface of the gold coated chip. Chips are thoroughly washed after step one, three and four. (B) The pH7 chip, center, represents two TMV1cys attachment spots showing the directed coassembly of D77K-HA onto attached TMV1cys under pH 7 buffer conditions. The pH 9 chip, left, shows how subsequently incubating a similar D77K-HA coassembled chip in pH 9 buffer leads to the disassembly and loss of the D77K-HA CP, while incubation in deionized water, right chip, shows no disassembly of D77K-HA CP (C) The center 0.2M NaCl chip shows the directed coassembly of R46G/E50K/E97G-FLAG onto surface attached TMV1cys under salt conditions. The deionized water chip, left, shows a similar co-assembled chip subsequently incubated under no-salt conditions, displaying the disassembly and loss of the R46G/E50K/E97G-FLAG CP from the TMV1cys. The pH 9 chip, right, shows disassembly of R46G/E50K/E97G-FLAG CP from TMV1cys does not occur in a pH dependent manner.

with its disassembly at low ionic strength conditions (Figure 3D). Combined these results indicate that carboxylate alterations can be used in the controlled assembly and disassembly of chimeric VLPs.

4. Surface-Bound Fabrication of Coassembled Nanoparticles. The ability of D77K-HA and R46G/E50K/E97G-FLAG CPs to coassemble onto a surface-attached TMV base layer in a condition-dependent manner was also investigated. For these studies, gold-coated silicon wafer chips were spotted with 3µl of 0.1mg/ml TMV1cys virus (Figure 4A). TMV1cys encodes a novel cysteine residue within its N-terminal arm that has been demonstrated to function in the attachment of the virus onto gold surfaces [4]. Specifically, the added cysteine thiol group is surface exposed only on the TMV rod ends, allowing for the formation of thiol – gold bonds that attach one end of the virus rod to the gold surface leaving the other end exposed for further modification. TMV1cys-spotted chips were incubated in 1ml of Tris buffer saline (0.2M NaCl), pH7 followed by the addition of 20ul of 0.5µg of D77K-HA CP, disassembled by dialysis in pH 9 Tris buffer or R46G/E50K/E97G-FLAG CP, disassembled by dialysis in pH 7 deionized water. Added CPs were incubated overnight at room temperature to permit coassembly onto surface-attached TMV1cys. Coassembled chips were incubated overnight in either Tris buffer saline (0.2M NaCl), pH 7 or pH 9, or with deionized water, pH 7. Chips were then washed and incubated in Tris buffer saline with primary tag specific antibody (FLAG or HA) followed by the addition of

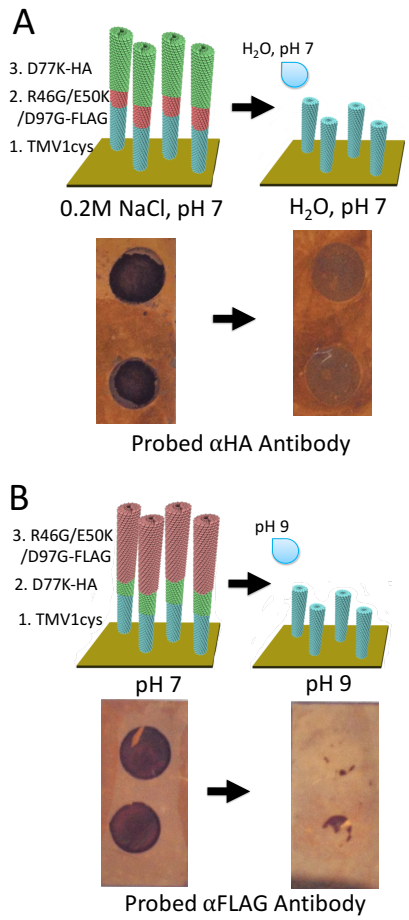

Figure 5. Layered assembly of carboxylate altered CPs. (A) Top panel diagram for the sequential assembly of, step 1, surface attached TMV1cys followed by, step 2, the addition and coassembly of R46G/E50K/E97G-FLAG CP in 0.2M NaCl, pH 7 buffer and then, step 3, coassembly of D77K-HA CP in pH7 buffer. Lower panel shows two gold coated chips each with two TMV1cys attachment spots. Sequentially assembled chips were probed with anti-HA antibody as described in Figure 6. The chip on the left was incubated in O.2M NaCl pH 7 buffer, conditions that promote the stability of both R46G/E50K/E97G-FLAG and D77K CPs. The chip on the right was incubated in deionized water pH 7, conditions that result in the disassembly of R46G/E50K/E97G-FLAG CP but not the D77K-HA CP. The inability to detect assembled D77K-HA CP on the deionized water treated chip indicates that disassembly of the R46G/E50K/E97G-FLAG CP layer also results in the loss of the D77K-HA CP layer. (B) Upper panel diagram for the sequential coassembly onto, step 1, surface attached TMV1cys, followed by, step 2, D77K-HA CP in pH 7 buffer and finally, step 3, coassembly with R46G/E50K/E97G-FLAG CP in 0.2MNaCl pH 7 buffer. Lower panel with two coassembled gold coated chips each with two TMV1cys attachment spots probed with anti-FLAG antibody. Prior to antibody incubation the chip on the left was incubated in O.2M NaCl pH 7 buffer, conditions that maintain the stability of both D77K-HA and R46G/E50K/E97G-FLAG CPs. The chip on the right was incubated in O.2M NaCl pH 9, conditions for the disassembly of D77K-HA CP but not the R46G/E50K/E97G-FLAG CP. The inability to detect assembled R46G/E50K/E97G-FLAG CP on pH 9 treated chips indicates that disassembly of the D77K-HA CP layer also results in the loss of the R46G/E50K/E97G-FLAG CP layer.

secondary alkaline phosphatase conjugated antibody and finally the addition of substrate, resulting in the production of a dark precipitant on the surface of the gold coated chip.

Results demonstrate both D77K-HA and R46G/E50K/E97G-FLAG CPs maintain their pH and ion concentration-dependent assembly and disassembly features when coassembled onto surface attached TMV1cys nanorods (Figure 4B and C). Importantly, surface assembled D77K-HA CP was only responsive to pH and not to ionic strength while assembly of the R46G/E50K/E97G-FLAG CP was affected only by ionic strength and not pH. Thus, these CPs maintain their solution assembly behaviors when coassembled on surface attached TMV1cys nanorods. Sequential assemblies composed of surface-attached TMV1cys coassembled first with either D77K-HA and second with R46G/E50K/E97G-FLAG CPs or first with R46G/E50K/E97G-FLAG and second D77K-HA CPs were also investigated as a means to control the layering of specific CPs. To confirm sequential assembly, individual chips were washed under buffer conditions that promote the disassembly of the first coassembled CP layer, deionized water for R46G/E50K/E97G-FLAG or pH 9 for D77K. Washed chips were then probed using antibodies against the second coassembled CP. Results demonstrate the sequential assembly of R46G/E50K/E97G-FLAG and D77K onto surface attached TMV1cys (Figure 5A and B). This layering is confirmed by the ability of wash conditions specific for the disassembly of the first assembled CP layer to remove the second CP layer (Figure 5A and B). Thus, the unique assembly behaviors of the R46G/E50K/E97G-FLAG and D77K CPs can be used to control the layering of functionally distinct CP assemblies.

Aim 2. Interfacing VLP patterned enzyme cascades onto electrodes. The integration of enzyme cascades onto device interfaces represents an under-investigated area that is critical to any future application of this science. To address this need, efforts in this aim investigated the use of our TMV-VLP vertical assembly system to position enzyme-patterned VLPs onto electrode surfaces.

1. An on-chip bioconjugation protocol has been developed for the assembly of enzymes onto electrode surface using TMV1cys. The molecular bioconjugations components of the assembly system are described in Figure 6. The assembly system is illustrated in Figure 7A, I) self-assembly of TMV1cys on Au surface was performed by introducing 20 µl of TMV1cys solution (0.2 mg/ml in 0.1 M phosphate buffer, pH7) followed by an overnight-incubation. Then a successive introduction of II) cross-linker (CL, maleimide-PEG-biotin) and III) streptavidin-conjugated GOx (GOx-STR) finalized the on-chip bioconjugation process. Each conjugation step lasted 5 hours at room temperature, and the electrode surface was rinsed 3X in PBS after each step to remove any unreacted/excess molecules. The simple conjugation reactions (thiol-maleimide binding and biotin-streptavidin binding) requiring only proper control over pH levels at room temperature in the absence of any catalytic reagents was essential for the facile bioconjugation process on-chip where control over reaction conditions (e.g. mixing between solutions, species concentrations)

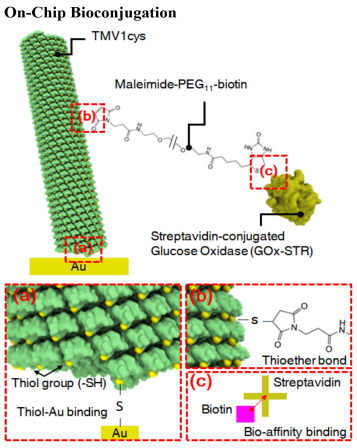

Figure 6. Illustrations of on-chip bioprinting process. All binding reactions occur sequentially in pH7 PBS at room temperature: (a) thiol-Au binding; (b) thiether covalent bond; (c) biotin-strepavidin based binding.

is not easily obtainable. The enzyme-immobilized electrodes have been evaluated in a horseradish peroxidase-luminol based colorimetric assay targeting H_2O_2 generated from the

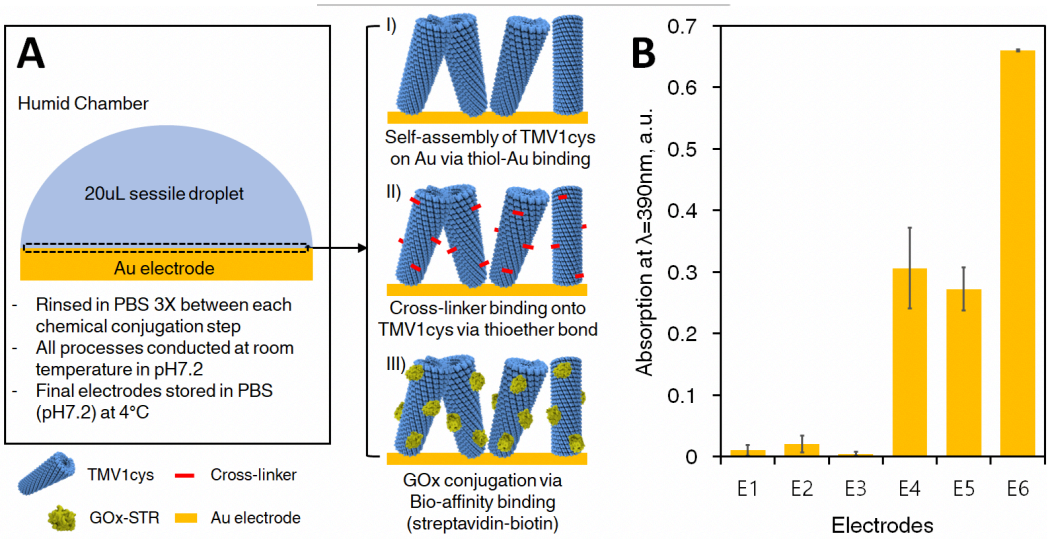

Figure 7. A. Illustration of the on-chip bioconjugation steps for enzyme immobilization via TMV1cys. B. A comparison of the optical absorption peaks from the colorimetric assays performed with the electrodes prepared in different conditions (E1: Bare Au, E2: Au/TMV1cys, E3: Au/TMV1cys/CL, E4: Au/GOx, E5: Au/TMV1cys/GOx, E6: Au/TMV1cys/CL/GOx, N=3).

enzymatic reaction carried by GOx. As shown in Figure 7B, the on-chip bioconjugation method resulted in a two-fold increase (E6) compared to the positive controls (E4 and E5) indicating the developed method is effective for high density GOx immobilization via TMV1cys.

Electrochemical characterization was performed 1) to understand the impact of the on-chip bioconjugation to the electrode kinetics and 2) to identify an effective charge transfer mechanism for the electrochemical conversion of the enzymatic reaction. Comparing the cyclic voltammetry (CV) obtained with a redox-couple mediator (ferri/ferro cyanide), the self-assembly of TMV1cys and the further conjugation of GOx with CL resulted in a corresponding decrease in charge transfer kinetics, showing an increasing separation between the redox peak potentials (Figure 8A). This is attributed to reduced ion accessibility to the electrode surface resulting in a decrease in the rate of electron transfers at the surface (Figure 8B). However, unlike the previously reported cases, where electrodes functionalized with smaller thiol molecules showed no electrochemical current response, the TMV1cys and the GOx bioconjugation steps still did not completely block the electrode surface, likely due to its nanoscale 3-D structure, ultimately allowing for electrochemical conversion of the enzymatic reactions.

The ferri/ferrocyanide redox couple was used as an electron mediator to convey enzymatic reaction-generated electrons to the Au electrodes (mediated-electron-transfer, MET). This was necessary as the direct-electron-transfer (DET) mechanism was not possible as indicated in Figure 9A - without the mediator molecule, no redox current peaks were observed in the CV curve in the presence of glucose. This is attributed to the use of planar Au as an electrode material which does not create a desirable arrangement of GOx on the conductive element - the cofactor/redox center, flavin adenine dinucleotide [5], of GOx should be directly accessible by the conductive medium with a stringent theoretical distance requirement (<1.5 nm). With the

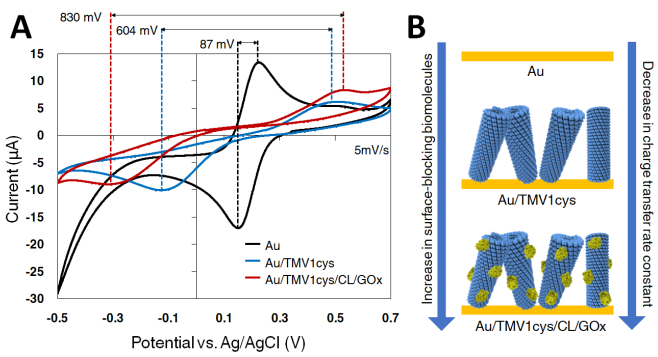

Figure 8. Impact of TMV1cys/CL/GOx conjugations on Au electrode to the electrode reaction kinetics: A. Cyclic voltammograms acquired from Au, Au/TMV1cys, and Au/TMV1cys/CL/GOx electrodes 1 mM Fe(CN)63-/4- solution in 1X PBS (pH7) showing increase in the redox peak separation and decrease in the redox current levels with respect to the on-chip GOx conjugation steps. B. Illustrations of the increase in the biomolecules (TMV1cys and GOx) with the sequential bioconjugation steps decreasing the accessibility of reactive species (e.g. Fe(CN)63-/4-) to the electrode surface causing relatively slower electrode charge transfer.

MET, an electrochemical response in CV corresponding to the glucose concentration was achieved, as shown in Figure 9, confirming successful electrochemical conversion of the enzymatic reaction. Figure 9C plots a calibration curve of the absolute reduction current corresponding to the glucose concentration levels (10 uM – 10 mM) demonstrating the excellent performance of the Au/TMV1cys/CL/GOx electrodes as glucose sensors. It should be noted that the reduction current was selected for determining the sensing capability as the oxidation currents showed rate-determined behavior with limited current levels compared to the reduction currents. Particularly, the results can be compared with a recent similar work by Bäcker et al. 2017 where they demonstrated glucose sensing with post-immobilization of TMV1cys/CL/GOx on Pt electrodes [6]. Comparing the current densities at the same glucose concentration, more than a 20-fold increase in current density (~3.4 μA/mm^2 vs. ~0.13 uA/mm^2 at 10 mM glucose) is achieved. The difference is most likely due to 1) the increased GOx immobilization density with high-density self-assembly of TMV1cys on Au surface and 2) the advanced generation of glucose sensing mechanism (2nd generation of glucose sensors relying on MET) incorporated in this work, whereas the previous work relied on direct reduction of H_2O_2, produced from the enzymatic reaction, on Pt electrodes (1st generation of glucose sensors). The combined results provide an effective on-chip bioconjugation strategy for high-density immobilization of GOx via TMV1cys and provides the fundamental understanding behind the electrode kinetics essential for monitoring enzymatic reactions on electrodes.

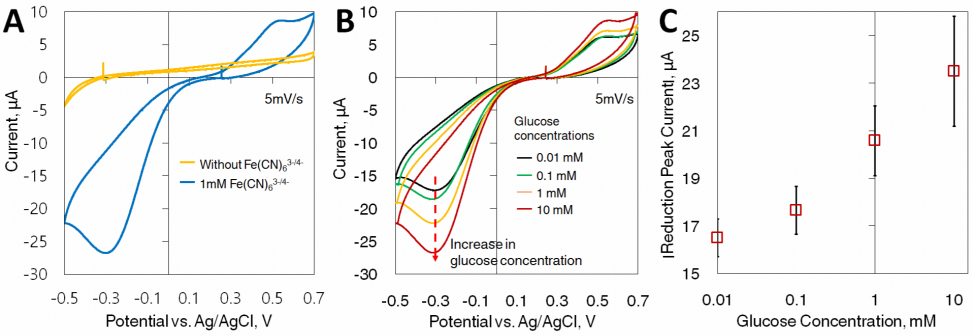

Figure 9. (a) Electrochemical characterizations (a) determining MET as an effective charge transfer mechanism and (b) demonstrating the change in redox current response corresponding to the glucose concentrations (10 uM -10 mM). (c) A calibration curve is generated using absolute reduction current peaks to highlight the excellent glucose sensing capability (N=3).

2. A second approach investigated for the attachment of functional proteins to the TMV VLPs involved the use of a split green fluorescent protein (GFP) system. In this system the 11 beta-sheet segments of GFP are split into two components, one containing beta-

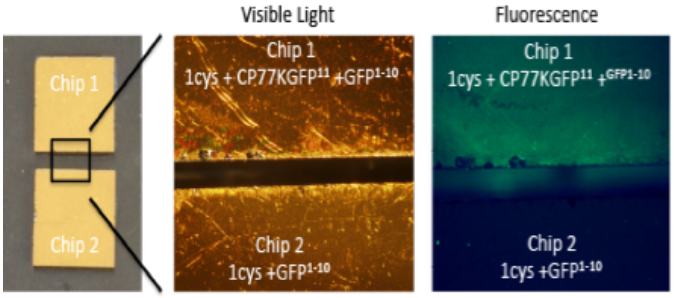

Figure 10. Chip based split GFP chimeric nanorod assembly system. Split GFP system, top chip assembled with all components necessary for fluorescence; bottom chip assembled minus the D77K-GFP11 component.

sheet segments 1-10, which were expressed as a hexa-his protein for Ni^{2+} column purification and a second peptide containing just the number 11 beta-sheet segment, which we genetically fused to the C terminus of the D77K subunit open reading frame to produce D77K-GFP11. TMV1cys assembled chips were incubated as described in Figure 10 with D77K-GFP11 to promote chimeric nanorod assembly. Subsequently these chimeric nanorods were incubated with purified GFP1-10 protein, which binds to the D77K displayed GFP11 beta sheet segment to complete the fluorescent protein. GFP1-10 binding is confirmed via fluorescence as shown in Figure 10. As the GFP1-10 peptide can be genetically fused with another functional peptide this assembly system provides a means to potentially monitor the assembly of functional peptides onto the TMV scaffolds through the use of fluorescence.

Aim 3: <u>Microfluidically controlled compartmentalization of TMV-VLP patterned enzymatic cascades</u>. The compartmentalization of enzymatic cascades is an essential trait within biological systems, functioning to concentrate components of the cascade while promoting the efficient conversion of substrate and reactant intermediates. Efforts in this aim will investigate microfluidic systems for the compartmentalization of VLP-patterned enzymatic cascades.

Progress:

The ability to bio-print both TMV scaffolds as well as enzymes and cross-linkers as means to control the on-chip compartmentalization of these reagents at the microscale level was the main focus of this objective. To achieve this goal a fully automated, programmable 3D electro-bio-printer was developed by revising a standard fused-deposition modeling (FDM) 3-D printer (Anycubic kossel delta), with custom-designed bio-ink cartridges and liquid extrusion nozzles. As shown in Figure 11a the printer is compatible with a standard 4-inch wafers where microfluidic devices will be fabricated and can be installed with 2-3 nozzles/cartridges at a time to implement sequential molecular on-chip assemblies that incorporate cycles of "print-incubate-rinse-print-incubate" - needed for sequential on-chip conjugation of the TMV-VLP and enzymes. Figure 11b shows the custom syringe-based nozzles integrated with lead screw connected to a stepper motor. This can dispense bio-ink volumes in 10-100 nL range per printing, determined based on the lead screw control and syringe volume, and repeat "extrude-retract" for an integrated rinsing procedure between each assembly steps.

This "print-assembly" approach was directed onto micropillar (μPA) electrodes created by negative photoresist (NR-9 1500py) and deep reactive ion etching. This was followed by surface passivation with 500 nm PECVD SiO_2 at 300 C, and completed with sputter deposition of Cr (30 nm)/Au (120 nm). Print-assembly onto these μPA electrodes involved EBP of TMV1cys nanorods directly onto the gold coated electrodes followed by successive introductions of cross-linker maleimide-PEG_{11}-biotin and glucose oxidase–streptavidin (GOx-STR) (Figure. 12). Results demonstrated the uniform coating of TMV1cys and conjugated GOx enzyme along the length of the μPAs with a 2.2-fold higher colorimetric response in comparison to controls. These

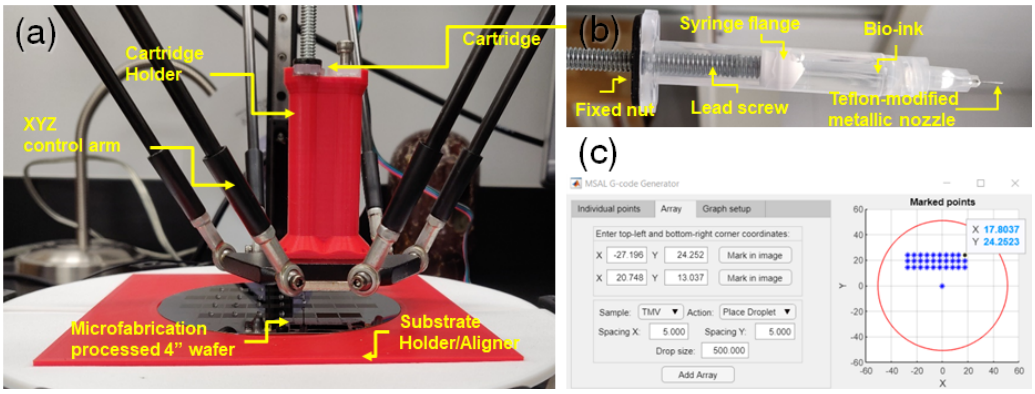

Figure 11. Wafer-scale multi-nozzle 3-D electro-bio-printer with designated graphical user interface. (a) Both the sample stage/aligner and the bio-ink cartridge holder have been custom-designed using a CAD software and 3-D printed using FDM technology. (b) A standard syringe and nozzles used for bioprinters have been integrated with a linear motor actuated lead screw to enable controlled-extrusion of liquid samples/bio-inks. (c) The MATLAB-based GUI allows programming of the printing process including print, retract, and rinse operations with parameters including print volume, patterns, sequence and location

findings indicate that the TMV1cys and the print-assembly crosslinking chemistry was effective for improved enzyme immobilization.

As a step toward understanding the power performance of the Au/TMV1cys/CL/GOx electrodes in this study, the impact of TMV1cys self-assembly on planar Au electrodes was investigated for its charge transfer kinetics using cyclic voltammetry (CV:scan range: -0.1 - 0.6 V vs. Ag/AgCl, scan rate: 100mV/s). Figure 13 shows top-down SEM images of the Au electrodes with different densities of TMV1cys particles, achieved by using different TMV1cys solution concentrations in the self-assembly step. Figure 13b and 13c show the cyclic voltammograms at different TMV1cys surface densities and the electrode charge transfer-associated parameters, respectively. The correspondence of both the incremental peak potential separations and the decrease in current peak intensities, at the same scan rate (100 mV/s), to the surface density implies a decrease in electrode kinetics; the rate of electron transfer at the

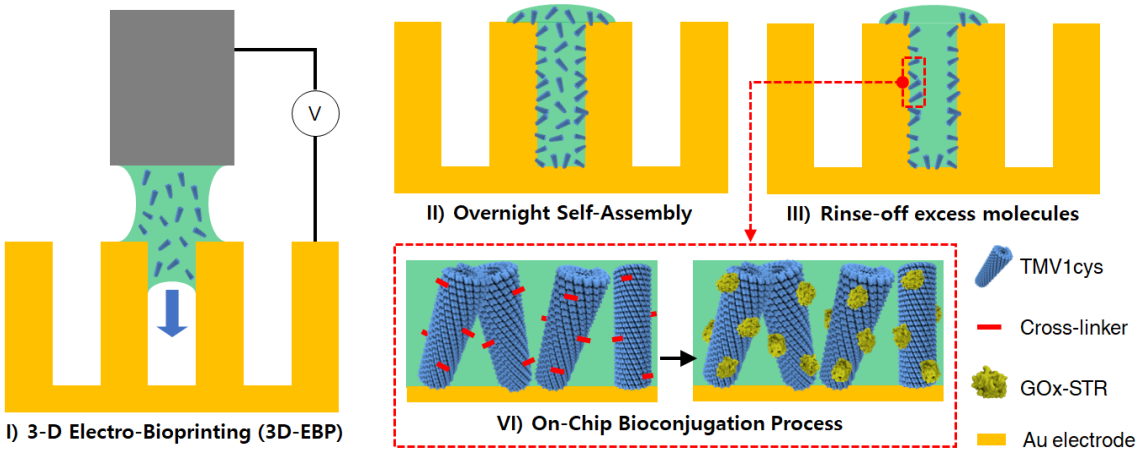

Figure 12. Illustration of the 3D-EBP incorporated bioconjugation process on Au-coated Si μPA electrodes.

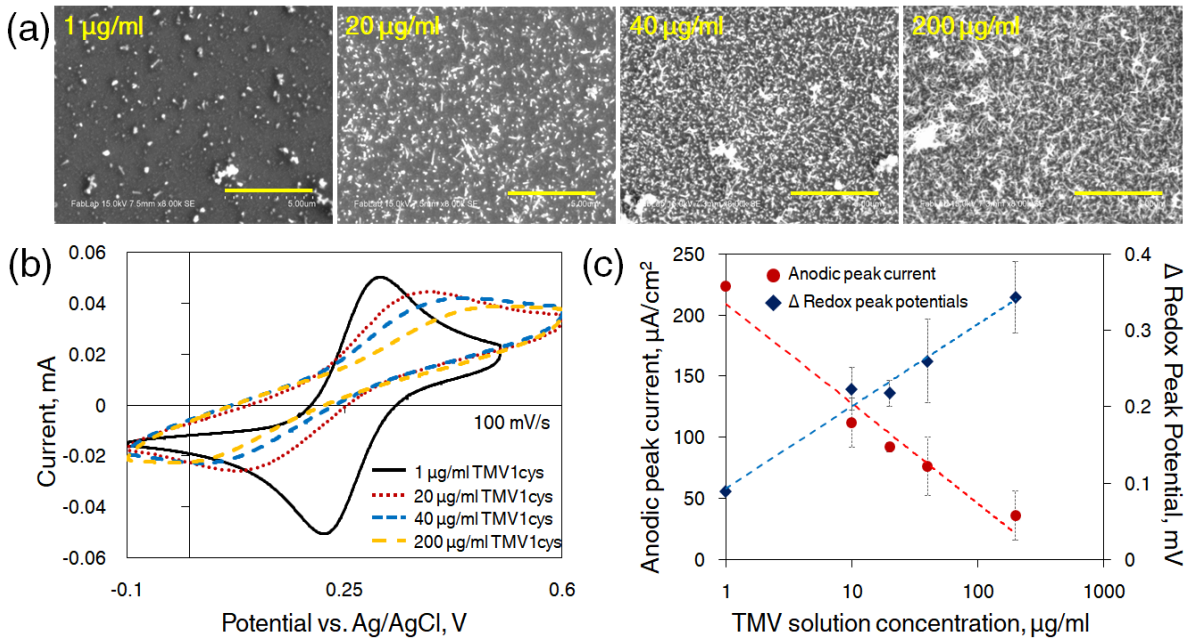

Figure 13: Impact of TMV1cys self-assembly on electrode kinetics: (a) Top-down SEM images of Au electrodes with different densities of self-assembled TMV1cys particles (scale bar: 5µm, the images are taken after electroless Ni coating). (b) Cyclic voltammograms acquired from the four different electrodes in 1 mM $Fe(CN)_6^{3-/4-}$ solution in 1X PBS (pH7) and (c) analysis of the change in peak potential separation and oxidation peak current density showing shift in electrode kinetics from a diffusion-limited to a rate-determined process (n=3).

electrodes is likely reduced due to the surface passivation with TMV1cys. The range of the peak separations and the comparable levels between the oxidation and reduction peak intensities imply that the charge transfer reaction is in a quasi-reversible regime, indicating that the resulting currents are predominately governed by the rate of electron transfer rather than a diffusion-limited process [7]. Compared to previous studies, using smaller organo-thiol molecules for formation of self-assembled monolayers (SAM) of organic molecules, this result indicates that there are "pin-holes" between the assembled TMV1cys particles or via the central channels of TMV1cys, allowing redox species to access the electrode surface for reactions, In contrast, complete coverage achieved using the smaller thiol molecules results in no electrochemical current response [8, 9]. Combined these findings suggest that the tube-like structure of the TMV rod provides a unique nano-structure for redox transport.

References:

1. Lu, B., G. Stubbs, and J.N. Culver, *Carboxylate interactions involved in the disassembly of tobacco mosaic tobamovirus.* Virology, 1996. **225**(1): p. 11-20.
2. Namba, K., R. Pattanayek, and G. Stubbs, *Visualization of protein-nucleic acid interactions in a virus - refined structure of intact tobacco mosaic virus at 2.9 A resolution by X-ray fiber diffraction.* Journal of Molecular Biology, 1989. **208**(2): p. 307-325.
3. Stryer, L., J.M. Berg, and J.L. Tymoczko, *Biochemistry*. 5th ed. 2002, New York: Freeman, W.H.
4. Royston, E., A. Ghosh, P. Kofinas, M.T. Harris, and J.N. Culver, *Self-assembly of virus-structured high surface area nanomaterials and their application as battery electrodes.* Langmuir, 2008. **24**(3): p. 906-12.
5. Lochon, F., L. Fadel, I. Dufour, D. Rebière, and J. Pistré, *Silicon made resonant microcantilever- Dependence of the chemical sensing performances on the sensitive coating thickness.* Materials Science and Engineering C, 2006. **26**: p. 348-353.
6. Backer, M., C. Koch, S. Eiben, F. Geiger, F. Eber, H. Gliemann, A. Poghossian, C. Wege, and M.J. Schoning, *Tobacco mosaic virus as enzyme nanocarrier for electrochemical biosensors.* Sensors and Actuators B-Chemical, 2017. **238**: p. 716-722.
7. Elgrishi, N., K.J. Rountree, B.D. McCarthy, E.S. Rountree, T.T. Eisenhart, and J.L. Dempsey, *A Practical Beginner's Guide to Cyclic Voltammetry.* Journal of Chemical Education, 2018. **95**(2): p. 197-206.
8. Love, J.C., L.A. Estroff, J.K. Kriebel, R.G. Nuzzo, and G.M. Whitesides, *Self-assembled monolayers of thiolates on metals as a form of nanotechnology.* Chemical Reviews, 2005. **105**(4): p. 1103-1169.
9. Tlili, A., A. Abdelghani, S. Hleli, and M.A. Maaref, *Electrical characterization of a thiol SAM on gold as a first step for the fabrication of immunosensors based on a quartz crystal microbalance.* Sensors, 2004. **4**(6-7): p. 105-114.